J. Plasma Physics (2013), vol. 79, part 5, pp. 751–757. © Cambridge University Press 2013
doi:10.1017/S0022377813000391

Set of wires to simulate tokamaks with poloidal divertor

T. KROETZ[1], CAROLINE G. L. MARTINS[2], M. ROBERTO[2] and I. L. CALDAS[3]

[1]Universidade Tecnológica Federal do Paraná, Pato Branco, Paraná, 85503-390, Brazil
[2]Departamento de Física, Instituto Tecnológico de Aeronáutica, São José dos Campos, São Paulo, 12228-900, Brazil
(marisar@ita.br)
[3]Instituto de Física, Universidade de São Paulo, 05315-970, São Paulo, Brazil

(Received 22 December 2012; revised 19 February 2013; accepted 18 March 2013; first published online 12 April 2013)

Abstract. Simple wire models have been proposed to simulate magnetic configurations in tokamaks. Here we consider electric currents in five parallel infinite wires to obtain double-null magnetic surfaces with specific choices of magnetic axis positions, triangularity, and elongation. As an example, we choose the position and the electric current of each wire to obtain magnetic surfaces similar to those expected in the tokamak international thermonuclear experimental reactor. Moreover, we also integrate the perturbed field line differential equation to simulate chaotic layers near the hyperbolic points and deposition patterns at the divertor plate observed in tokamaks. To simulate that, we add to the model a perturbing error field, due to asymmetries in the tokamak coils, and introduce a random collisional term to the field line mapping to reproduce escape pattern alterations due to particle collisions.

1. Introduction

Tokamaks with poloidal divertors have substantially improved the magnetic confinement of plasmas for thermonuclear controlled fusion (Janeschitz 2007) and this good performance will be tested in the future international thermonuclear experimental reactor (ITER). The magnetic configuration of tokamaks with divertors contains a toroidal magnetic surface separating closed field lines on nested surfaces from open field lines hitting the divertor plates (Boozer and Rechester 1978). Moreover, the brake of symmetry due to error fields and plasma oscillations create chaotic field lines around the separatrix (Wingen et al. 2009a).

Numerical field line calculations in diverted plasmas based on numerical equilibria reconstructions are well known in the literature (Evans et al. 2002). However, computational codes that integrate magnetic field line equations in tokamaks and describe both open and chaotic field lines near poloidal divertors are time-consuming and generate a great computational cost (Casper et al. 2007; Brix et al. 2008; Wingen et al. 2009b). Basic dynamical properties of field lines can be well described by simple models that have been introduced to reproduce the main magnetic field line dynamics near the separatrix. Generally, simple models consider a set of coils or wires to reproduce fields similar to those typical of magneto-hydrodynamic (MHD) equilibrium in tokamaks.

The magnetic field of two infinite wires was introduced in 1978 to calculate the width of the scrape-off layer of a divertor tokamak (Boozer and Rechester 1978). Equilibrium models using two and three infinite wires were used to study the chaotic layer formation due to error fields in single-null (one X-point) (Pomphrey and Reiman 1992) and double-null (two X-points) (Reiman 1996) divertor tokamaks, respectively. The particle drift orbits were obtained in Daybelge and Yarim (1999) for a model of three circular coils in the presence of non-axisymmetric magnetic field perturbations. A comparison between the chaotic layer formation using a two-wire model and a discrete map was investigated in Ali et al. (2004, 2008). A single-null equilibrium plasma model, composed by three infinite wires, was used in Abdullaev et al. (2006) to implement a method of canonical mapping near the separatrix in presence of magnetic perturbations created by pairs of loop coils with opposite flowing currents.

In this work we use a set of five parallel infinite wires conducting electric currents to describe equilibrium magnetic surfaces of double-null divertor tokamaks. This number of wires is sufficient to reproduce the cross-section of an arbitrary choice of magnetic configuration, depending on the wire positions and their currents. In comparison with Pomphrey and Reiman (1992) and Reiman (1996), our configuration with five wires introduces the possibility to adjust the triangularity and elongation of the flux surfaces. Thus, our model can better analyze lines transport similar to those observed in more precise descriptions of tokamak plasma equilibrium with divertors (Wingen et al. 2009a, b).

We show the model versatility by creating surfaces with similar topology of ITER surfaces. This simple model reproduces quite well ITER-like magnetic topology capturing some aspects of the magnetic field line

dynamics of plasma region near the separatrix, but not in the plasma core.

Non-axisymmetric magnetic perturbations destroy the magnetic separatrix creating homoclinic tangles, leading to the formation of a layer of chaotic field lines (Joseph et al. 2008). The structure of this chaotic layer determines the pattern of magnetic footprints on divertor plates (deposition patterns) and directly interferes on heat flux transport (Joseph et al. 2008). To study the field line escape patterns near the destroyed separatrix, we introduce perturbations on the equilibrium created by resonant magnetic perturbations by error fields due to asymmetries on external coils (Pomphrey and Reiman 1992; Reiman 1996) and an additional noise to simulate the collisional diffusion of particles (Beaufume et al. 1990). We solve numerically the perturbed magnetic field line differential equation to investigate the effect of magnetic perturbations on chaotic layer formation and deposition patterns at the divertor plate.

We introduce the model of five infinite wires in Sec. 2. Numerical results on equilibrium and perturbed magnetic surfaces are presented in Secs. 3 and 4 respectively. We present numerical examples of escape pattern typical of those computed for tokamaks in Sec. 5. Finally, in Sec. 6 we present the conclusions.

2. The model

The magnetic field equations produced by a set of N infinite wires are written in rectangular coordinates as

$$B_x(x,y) = \sum_{i=1}^{N} \frac{\mu_0 I_i}{2\pi} \frac{(y-y_i)}{(x-x_i)^2+(y-y_i)^2}, \quad (1)$$

$$B_y(x,y) = \sum_{i=1}^{N} \frac{\mu_0 I_i}{2\pi} \frac{-(x-x_i)}{(x-x_i)^2+(y-y_i)^2}, \quad (2)$$

where I_n and (x_n, y_n) are the electric current and position of the nth wire. In this work we use $N = 5$ wires, where one of them represents the plasma current (I_p) and the other four reproduce a desirable plasma shape in tokamaks. The position (x_p, y_p) of I_p coincides with the magnetic surface axis at $z = 0$.

The magnetic field created by five wires is in the plane (x, y). To model the toroidal geometry, we must introduce periodicity in the z-direction. Thus, to reproduce the tokamak field we have to add the vertical field created by a solenoid. Therefore, the z-component of the toroidal field generated by the external coils is given by

$$B_z(x) = \frac{R_0 B_0}{x}, \quad (3)$$

where R_0 is the major radius of the torus (or geometric axis) and B_0 is the toroidal field at the geometric axis. Thus, for $x = R_0$, $B_z(R_0) = B$.

The equilibrium magnetic surfaces are defined as surfaces with field lines satisfying the condition $\vec{B}.\vec{\nabla}\psi = 0$, where

$$\psi(x,y) = \frac{\mu_0 I_p}{2\pi} \ln\left(r_p \prod_{n=2}^{N} r_n^{\frac{I_n}{I_p}} \right). \quad (4)$$

Table 1. Wire positions and current values of our model.

n	x_n (m)	y_n (m)	I_n (MA)
1. (plasma)	6.41	0.513	15.00
2.	3.72	−7.580	15.90
3.	3.20	8.600	16.28
4.	2.45	0.513	−5.69
5.	10.00	0.513	−4.60

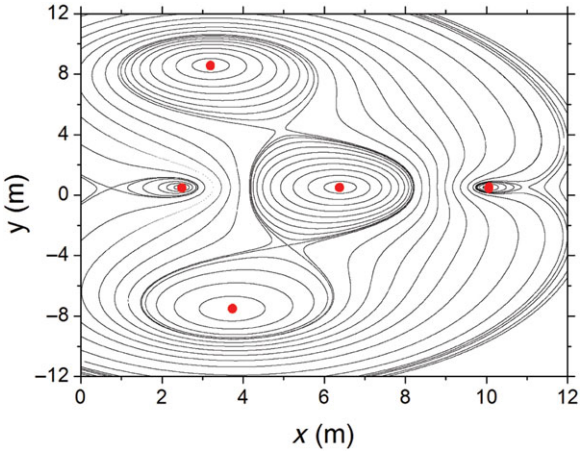

Figure 1. (Colour online) Magnetic surfaces at inner and outer separatrixes. The red points indicate each wire position.

The function $\psi$is the magnetic flux passing through a plane along the z-direction extending from the magnetic axis out to the generic point (x, y). The distance of the generic point (x, y) from the position (x_n, y_n) of the conductor I_n is defined by $r_n = [(x-x_n)^2 + (y-y_n)^2]^{1/2}$.

Interpreting the z-coordinate as an independent variable we can write the differential equation of the field lines $\vec{B} \times \vec{dl} = 0$ as

$$\frac{dx}{dz} = \frac{B_x}{B_z}; \quad \frac{dy}{dz} = \frac{B_y}{B_z}. \quad (5)$$

In Sec. 3, to study the magnetic configuration with the wires model, we integrate numerically (5) using the Runge–Kutta method.

3. Numerical results: magnetic surfaces

In our model, to represent equilibrium magnetic surfaces of ITER configuration, with the major parameters of ITER listed in Janeschitz (2007), we choose the parameters of currents and positions of wires listed in Table 1.

Wire 1 represents the plasma current and its position coincides with the magnetic surfaces axis. The major role of wires 2 and 3 is to create the lower and upper X-points, respectively. The positions of lower and upper X-points are in different separatrixes. The negative currents in wires 4 and 5 compress the left and right sides of magnetic surfaces and allow us to model the desired elongation of surfaces. The wire currents and positions are chosen according to the values of ITER parameters.

Figure 1 shows the positions of wires represented by red points, with the surfaces generated by them.

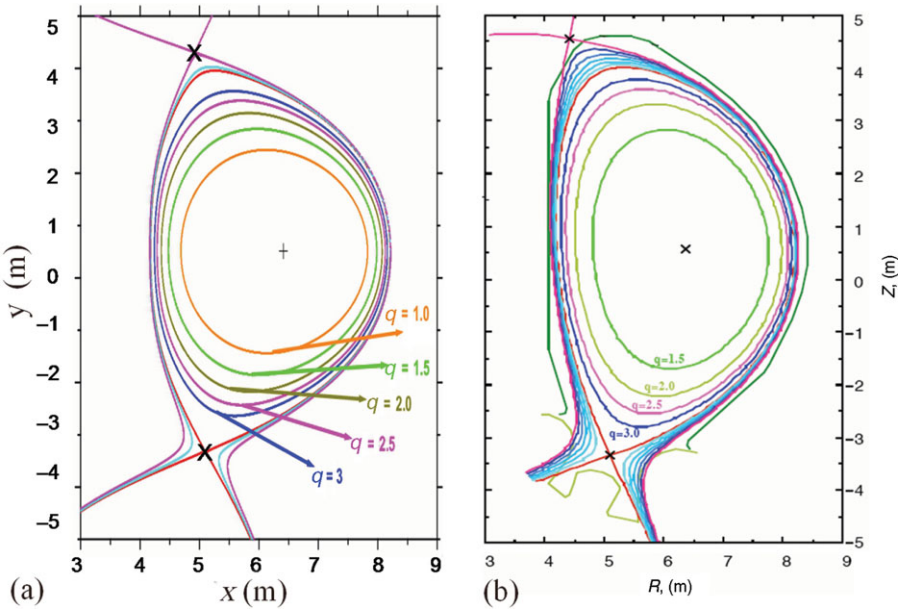

Figure 2. (Colour online) (a) Magnetic surfaces obtained from the model with colors representing different values of $\psi(x, y)$; (b) ITER magnetic surfaces (extracted from Janeschitz (2007). Average safety factor values, q, are indicated in both figures.

Figure 2(a) shows magnetic surfaces indicated by colors representing different values of $\psi(x, y)$ calculated by our model. Figure 2(b), extracted from Janeschitz (2007), shows magnetic surfaces obtained for the magnetic configuration of ITER. In both figures the values of the safety factor, q (defined below), for magnetic surfaces internal to the separatrixes are indicated. We can verify a good agreement between the magnetic surfaces and safety factor profiles calculated by our model and those designed for ITER.

Each magnetic surface has a well-defined pitch related to the so-called rotational transform, which is the average poloidal angle swept by a field line after one complete toroidal turn. In the present model, the poloidal angle is the angular displacement performed on the x–y plane by a straight line that connects the magnetic axis to a specific magnetic field line. For tokamaks the inverse of rotational transform is the safety factor used to characterize the line topology.

To obtain the safety factor profile of magnetic surfaces, we integrate the system of (5) for many initial conditions lying on a horizontal line connecting the magnetic axis to the right side of the separatrix. We consider that a field line completes m toroidal turns if $z = 2m\pi R_0$. Thus, on rational surface with a safety factor $q = m/n$, the periodic field lines perform m toroidal and n poloidal turns.

Figure 3 presents the safety factor profile calculated from our model for initial conditions indicated on the x-axis (with $y = 0$). In this figure we can identify the positions of two surfaces with infinite safety factors. These surfaces correspond to two separatrixes as shown in Fig. 1. In a magnetic system, hyperbolic points correspond to the positions with null poloidal magnetic field ($B_x$and $B_y = 0$) and, consequently, to safety factor values

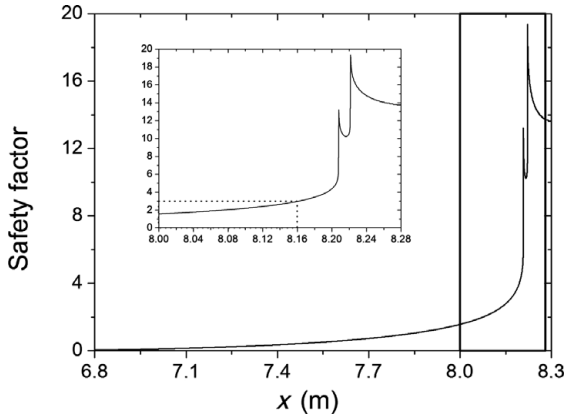

Figure 3. Safety factor profile for the magnetic surfaces of Fig. 1. The rectangle indicates the region amplified in the insert. The dotted line in the insert indicates the value $q = 3$ corresponding to a magnetic surface containing the point $x = 8.16$ m, which corresponds to the last closed surface.

that go to infinity. The dotted line in Fig. 3 indicates the value $q = 3$ corresponding to a magnetic surface containing the point $x_0 = 8.16$ m, which corresponds to the last closed surface. We also show a rectangle in Fig. 3, which includes initial conditions in the external region ($x > 8.16$), namely the plasma edge and the scrape-off layer. Profiles similar to the one shown in Fig. 3 are expected in the tokamak ITER whose external magnetic surfaces have safety factor greater than three.

4. Numerical results: perturbed magnetic surfaces

To investigate the effect of magnetic perturbations on the chaotic layer formation, we perturb the field line equations by adding field components described by a

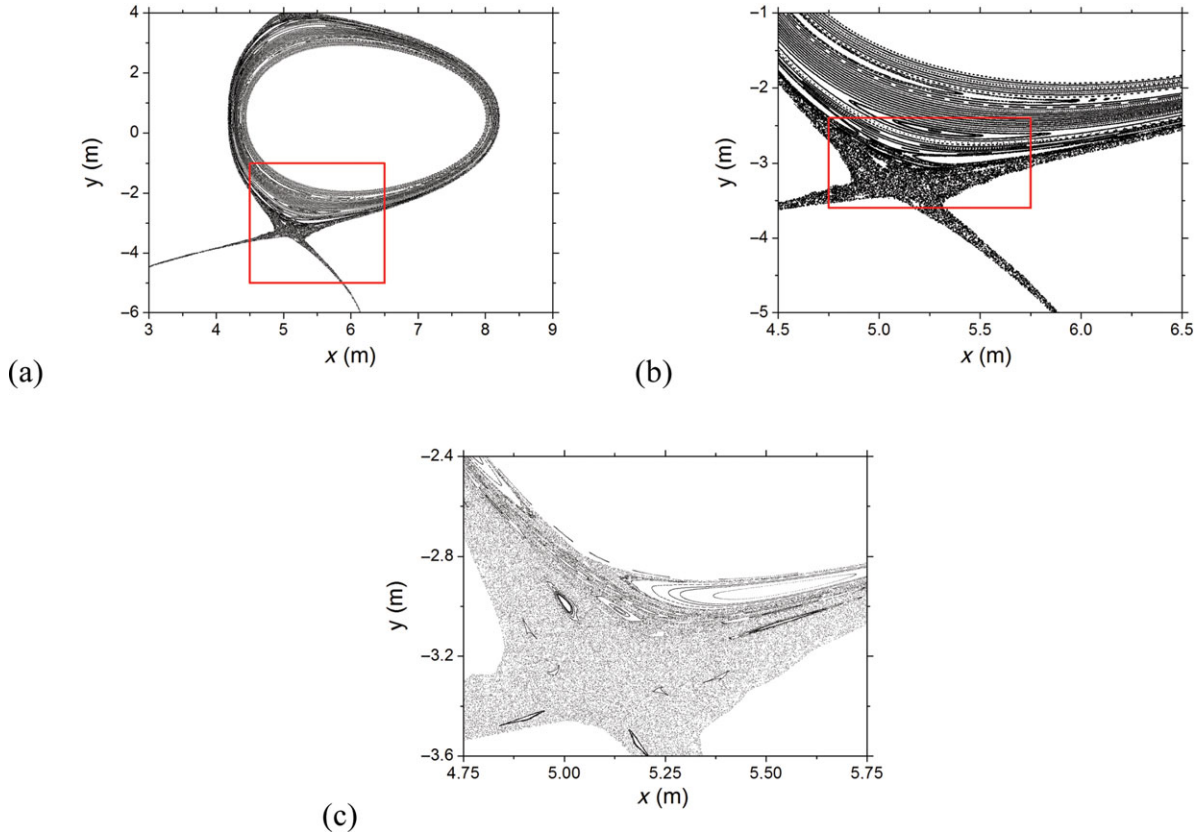

Figure 4. (Colour online) (a) Chaotic layer due to an error field with perturbation parameter $\varepsilon = 2 \times 10^{-4}$. (b) Amplification of the red rectangle shown in (a). (c) Amplification of the red rectangle of (b) showing magnetic islands immersed in the chaotic layer.

model, proposed in Pomphrey and Reiman (1992), of error fields due to asymmetries on external coils. Thus, the perturbed line equations are

$$\frac{dx}{dz} = \frac{B_x + B_x^{(p)}}{B_z + B_z^{(p)}}; \quad \frac{dy}{dz} = \frac{B_y + B_y^{(p)}}{B_z + B_z^{(p)}}, \tag{6}$$

where $B_x^{(p)}$, $B_y^{(p)}$, and $B_z^{(p)}$, the rectangular components of the perturbing field, can be written as

$$\vec{B}(p) = \varepsilon B_0 \nabla \chi \tag{7}$$

with

$$\chi = R_0 \exp\left[\frac{(x - x_p)}{R_0}\right] \cos\left(\frac{z}{R_0}\right). \tag{8}$$

Then the components are

$$B_x^{(p)} = \varepsilon B_0 \exp\left[\frac{(x - x_p)}{R_0}\right] \cos\left(\frac{z}{R_0}\right); \quad B_y^{(p)} = 0; \quad \text{and}$$

$$B_z^{(p)} = -\varepsilon B_0 \exp\left[\frac{(x - x_p)}{R_0}\right] \sin\left(\frac{z}{R_0}\right). \tag{9}$$

Fourier decomposition of error fields of Joint European Torus (JET) tokamak shows that the amplitude of perturbation can be estimated in $\varepsilon \approx 10^{-4}$ (Pomphrey and Reiman 1992; Reiman 1996).

We integrate the perturbed equations, with perturbation parameter $\varepsilon = 2 \times 10^{-4}$, and obtain Fig. 4(a) with a chaotic layer around the lower hyperbolic point. The magnetic field lines are no longer closed and eventually reach the inner part of the chamber following the lines leaving the X-point. These lines finish their trajectories at the divertor plate. In Figs. 4(b) and (c), it is possible to observe magnetic islands immersed in the chaotic layer. These islands play an important role on the field line escape (Kroetz et al. 2008).

5. Escape patterns

In this section we consider our model to calculate the field line escape to a divertor plate displayed horizontally at the position $y_f = -4.5$m. As the particles follow the field lines, the obtained escape structure should be closely related to the measurable plasma particle deposition profile on divertor plate.

To evaluate the considered field line escape, we calculate the connection length, which is the number of toroidal turns, m, performed by a field line until it reaches the plate. The magnetic field line is integrated forward and backward in z, for initial conditions in a box with $4.75 \leqslant x_0 \leqslant 5.70$ and $-3.80 \leqslant y_0 \leqslant -2.60$, until it reaches the plate at the position (x_f, y_f, z_f).

Figure 5(a) shows the connection length for the system with perturbation parameter $\varepsilon = 2 \times 10^{-4}$. The largest connection lengths are obtained from initial conditions near the broken separatrix. Figure 5(b) is an amplification of the rectangle indicated in Fig. 5(a) and reveals a structure of the connection length map similar to the

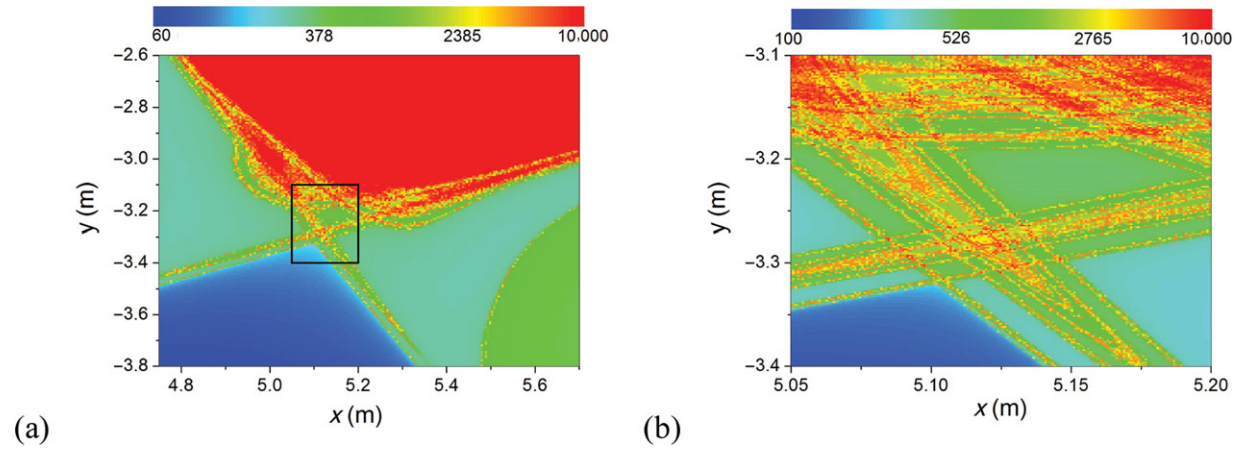

Figure 5. (Colour online) Connection lengths with perturbation parameter $\varepsilon = 2 \times 10^{-4}$ where the number of toroidal turns, m, is represented by the color scale displayed in logarithmic scale. (a) The connection lengths correspond to each initial condition in the Poincaré map. The rectangle indicates the area amplified in (b). (b) Amplification of (a) close to the X-point.

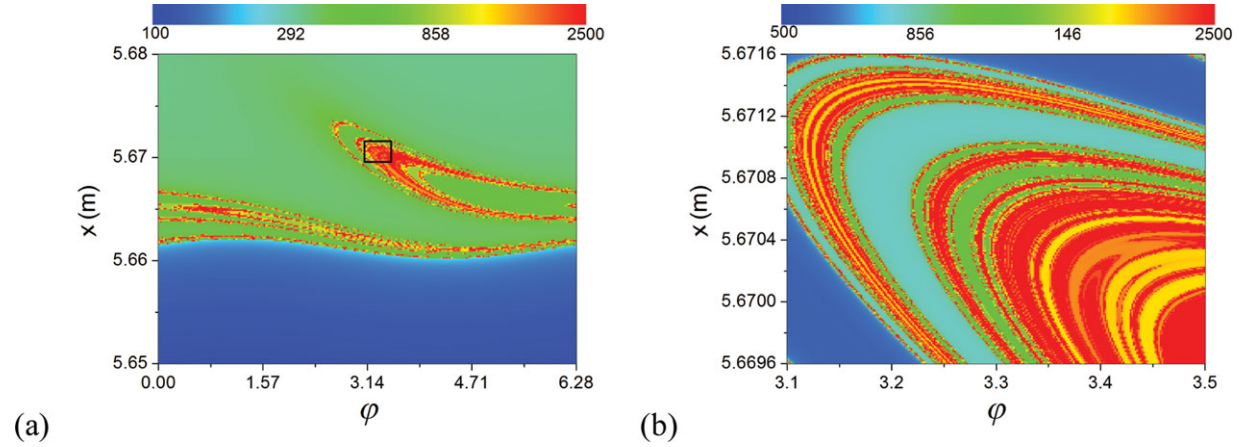

Figure 6. (Colour online) Footprints with perturbation parameter $\varepsilon = 2 \times 10^{-4}$. The colors are in logarithmic scale. (a) Places on the divertor plate, located at $y_f = -4.5$m, where magnetic field lines started. The colors indicate the connection length of each field line. (b) Amplification of the rectangle indicated in (a) reveals an inhomogeneous field line striking the divertor plate.

homoclinic tangle of stable and unstable manifolds that come from a hyperbolic fixed point (da Silva et al. 2002; Roeder et al. 2003; Wingen et al. 2009a). This kind of structure has been observed using computational codes that simulates escape patterns in Schmitz (2008).

As the system is periodic in z, we relate the z-coordinate with the toroidal angle $\varphi_f = z_f/R_0$. It allows us to calculate the footprint, which is the set of strike points of field lines at the divertor plate. The magnetic field line is integrated backward in z, for initial conditions located at the divertor plate $y_f = -4.5$m for a box with $5.65 \leqslant x_0 \leqslant 5.68$ and $0 \leqslant \varphi_0 \leqslant 2\pi$ until it reaches the plate at the position (x_f, y_f, φ_f).

Figure 6(a) shows the footprint, and a zoom in the rectangle (Fig. 6(b)) reveals an inhomogeneous line striking the divertor plate. Similar results have been observed in sophisticated simulation codes (Jakubowski 2009; Wingen et al. 2009a). Successive zooms of Fig. 6(b) were performed and showed a complex distribution of field lines that escape to the plate, evidencing a fractal structure (Viana et al. 2010). This field line complex structure is essentially determined by the fractal structure of the homoclinic tangle in chaotic region (Viana et al. 2010).

A study of escape patterns using a symplectic approach that represents the magnetic geometry of DIII-D revealed that the fractal dimension of footprints increases with the amplitude of topological noise (Evans 1991) and error fields (Punjabi and Ali 2011). Moreover, the radial profiles of connection lengths, poloidal turns before striking the plate, diffusion coefficient of magnetic field lines, and average of safety factor also present self-similarity.

Inside the plasma particle, transport is not only determined by the magnetic field lines but also by collisions. So to estimate the particle escape pattern from the magnetic topology obtained from our model, we have to modify the field line equations to simulate how collisions divert particle center guide from the field line trajectories. Recently, it has been verified in a simple numerical model for particle collision that the chaotic saddle of the magnetic field and its manifolds

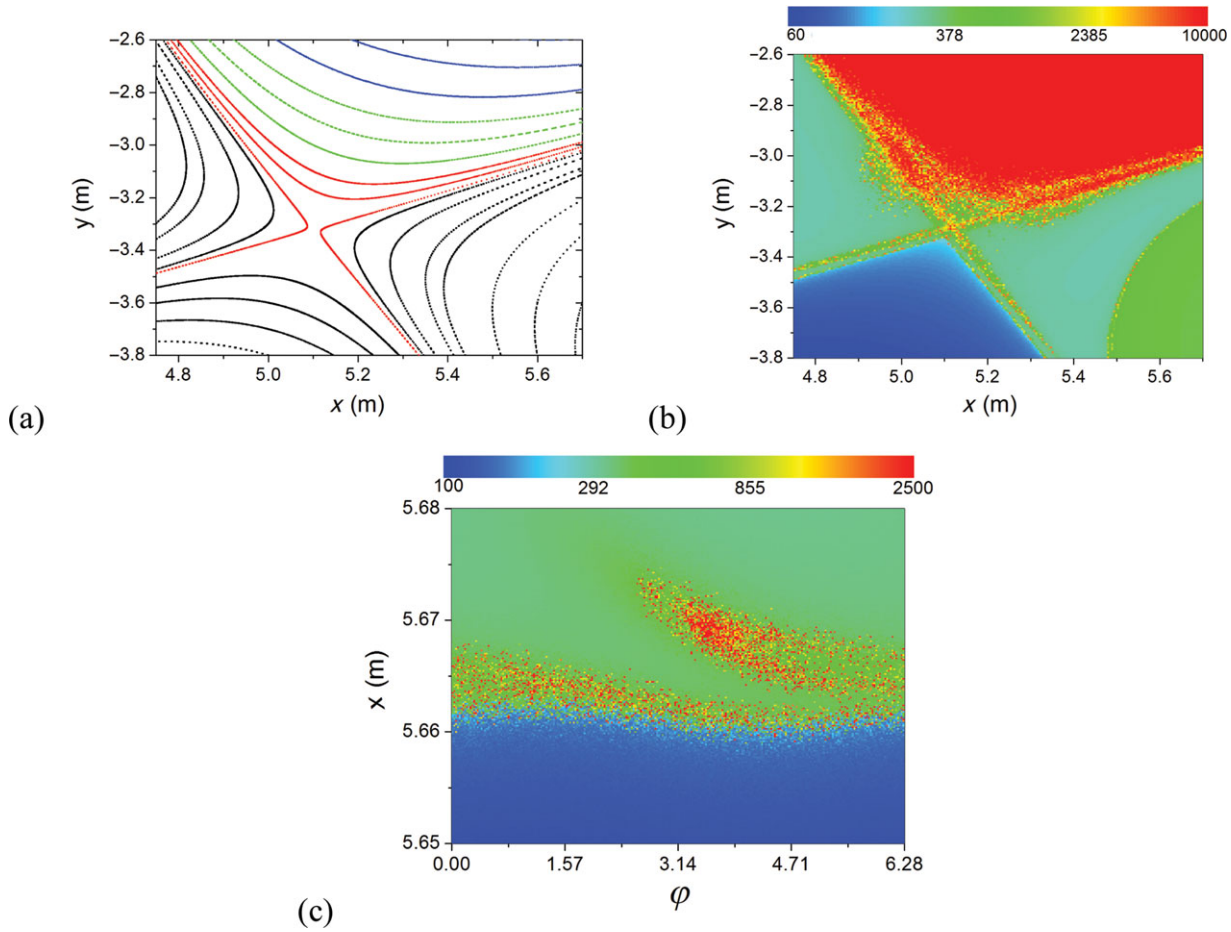

Figure 7. (Colour online) (a) Four regions, near the separatrix, with uniform noise amplitudes indicated by black, blue, green, and red colors. The black region is without noise; for the blue region,$\rho = 1 \times 10^{-4}$, for the green region,$\rho = 1 \times 10^{-3}$, and for the red region,$\rho = 5.5 \times 10^{-3}$. Connection lengths (b) and footprints (c) are obtained with noise for the perturbation parameter $\varepsilon = 2 \times 10^{-4}$; the number of toroidal turns, m, is represented by the color in logarithmic scale.

still govern the particle dynamics when collisions are included (Schelin et al. 2011). To do that, we add the effect of an additional noise in the system that simulates collisional diffusion of particles inside the plasma column. The effect of such noise is represented by adding a vector of random orientation to the magnetic field (Beaufume et al. 1990). Thus, the field line equation (6) becomes

$$\frac{dx}{dz} = \frac{B_x + B_x^{(p)}}{B_z + B_z^{(p)}} + \rho \sin(\theta_t);$$

$$\frac{dy}{dz} = \frac{B_y + B_y^{(p)}}{B_z + B_z^{(p)}} + \rho \cos(\theta_t), \qquad (10)$$

where ρ is the perturbation amplitude and $0 \leqslant \theta_t \leqslant 2\pi$ is a random phase. We choose ρ by analyzing the mean free path obtained for ITER (Artaud 2010).

However, as collisions are much dependent on plasma temperature to add noise in the system, we divide the region next to the separatrix in four, as shown in Fig. 7(a), roughly taking into account the expected non-uniform temperature profile in ITER. For the field lines located at the black region no noise is added. For the blue region the noise is added every time the field line reached the section$z = (\ell \times 2 \times \pi)$, with ℓ integer and noise amplitude $\rho = 1 \times 10^{-4}$. For the green region the noise is added every time the field line reached the section $z = (\ell \times \pi)$, with ℓ integer and noise amplitude $\rho = 1 \times 10^{-3}$. For the red region the noise is added every time the field line reached the section$z = (\ell \times (\pi/2))$, with ℓ integer and noise amplitude $\rho = 5.5 \times 10^{-3}$.

Figure 7(b) shows the influence of noise in the connection lengths and, comparing with Fig. 5(a), one can note a more inhomogeneous particle deposition around the vicinity of the separatrix. This observed inhomogeneity reflects the noisy perturbation added to the field lines. The main effect of the considered collisional term on the obtained connection lengths is due to the fact that particles no longer trace out the unstable manifold exactly, rather they disperse about it (Schelin et al. 2011). Figure 7(c) shows the preservation of the basic structure of the divertor footprint, as predicted from a much more detailed Monte Carlo fluid simulation code with realistic plasma parameters, given in Frerichs et al. (2012), as well as experimental results, as discussed in Schmitz (2008), which show that the particle flux, with multiple peaks on the divertor target plate, retains the basic structure of magnetic footprints. Thus, the

results shown in Figs. 7(b) and (c) suggest that the approach used in this model, with a right choice of noise amplitude, reproduces quite well the effects of collisions in comparison with experimental results and simulations from a more comprehensive treatment of collisional transport with realistic plasma parameters.

6. Conclusions

The presented infinite wire model is capable to reproduce single-null magnetic surfaces with specific choices of magnetic axis positions, triangularity, and elongation. The versatility of the model was exemplified recreating a magnetic configuration close to ITER equilibrium and similar safety factor profiles. Different kinds of perturbations can be easily used since the components of the perturbing magnetic fields are known. With this simple model of equilibrium configuration it is possible to study the qualitative characteristics of magnetic field line dynamics in the chaotic layer of a single-null divertor. A generic magnetic perturbation written as a Fourier expansion in terms of different resonant modes can also be used.

The continuous integration of magnetic field lines allows the obtaining of strike points of escaping field lines as well as their lengths, and they agree qualitatively with the results obtained with sophisticated computational codes. The addition of noise can simulate collisions between particles to create a more realistic scenario.

Acknowledgments

This work was made possible through partial financial support from the following Brazilian research agencies: FAPESP (São Paulo), CAPES, CNPq, and MCT-CNEN (Brazilian Fusion Network).

References

Abdullaev, S. S., Finken, K. H., Jakubowski, M. and Lehnen, M. 2006 Mappings of stochastic field lines in poloidal divertor tokamaks. *Nucl. Fusion* **46**, S113.

Ali, H., Punjabi, A. and Boozer, A. 2008 Stochastic layer scaling in the two-wire model for divertor tokamaks. *J. Plasma Phys* **75**, 303.

Ali, H., Punjabi, A., Boozer, A. and Evans, T. E. 2004 The low MN map for single-null divertor tokamaks. *Phys. Plasmas* **11**, 1908.

Artaud, J. F. et al. 2010 The CRONOS suite of codes for integrated tokamak modelling. *Nucl. Fusion* **50**, 043001.

Beaufume, P., Dubois, M. A. and Mohamed Benkadda, M. S. 1990 Diffusion in the noisy Chirikov-Taylor mapping. *Phys. Lett. A* **147**, 87.

Boozer, A. H. and Rechester, A. B. 1978 Effect of magnetic perturbations on divertor scrape-off width. *Phys. Fluids* **21**, 662.

Brix, M., Hawkes, N. C., Boboc, A., Drozdov, V., Sharapov, S. E. and JET-EFDA Contributors. 2008 Accuracy of EFIT equilibrium reconstruction with internal diagnostic information at JET. *Rev. Sci. Instrum.* **79**, 10F325.

Casper, T. A., Meyer, W. H., Pearlstein, L. D. and Portone, A. 2007 ITER shape controller and transport simulations. *Fus. Eng. Design* **83**, 552.

da Silva, E. C., Caldas, I. L., Viana, R. L. and San Juan, M. A. F. 2002 Escape patterns, magnetic footprints, and homoclinic tangles due to ergodic magnetic limiters. *Phys. Plasmas* **9**, 4917.

Daybelge, U. and Yarim, C. 1999 Pattern of ion bombardment on the poloidal divertor plates. *J. Nucl. Mat.* **269**, 809–811.

Evans, T. E. 1991 *Proceedings of the 18th European Conference on Controlled Fusion and Plasma Physics*, Berlin, Germany, Part II. Petit-Lancy, Switzerland: European Physical Society, p. 65.

Evans, T. E., Moyer, R. A. and Monat, P. 2002 Modeling of stochastic magnetic flux loss from the edge of a poloidally diverted tokamak. *Phys. Plasmas* **9**, 4957.

Frerichs, H., Reiter, D., Schmitz, O., Cahyna, P., Evans, T. E., Feng, Y. and Nardon, E. 2012 Impact of screening of resonant magnetic perturbations in three-dimensional edge plasma transport simulations for DIII-D. *Phys. Plasmas* **19**, 052507.

Jakubowski, M. W. et al. 2009 Overview of the results on divertor heat loads in RMP controlled H-mode plasmas on DIII-D. *Nucl. Fusion* **49**, 095013.

Janeschitz, G. 2007 The status of ITER; the ITER design review. *Paper presented to Town Meeting on APS-DPP Conference, ITER Design Review*, Orlando, FL.

Joseph, I., Evans, T. E., Runov, A. M., Fenstermacher, M. E., Groth, M., Kasilov, S. V., Lasnier, C. J., Moyer, R. A., Porter, G. D., Schaffer, M. J. et al. 2008 Calculation of stochastic thermal transport due to resonant magnetic perturbations in DIII-D. *Nucl. Fusion* **48**, 045009.

Kroetz, T., Roberto, M., da Silva, E. C., Caldas, I. L. and Viana, R. L. 2008 Divertor map with freedom of geometry and safety factor profile. *Phys. Plasmas* **15**, 092310.

Pomphrey, N. and Reiman, A. 1992 Effect of nonaxisymmetric perturbations on the structure of a tokamak poloidal divertor. *Phys. Fluids B* **4**, 938.

Punjabi, A. and Ali, H. 2011 An accurate symplectic calculation of the inboard magnetic footprint from statistical topological noise and field errors in the DIII-D. *Phys. Plasmas* **18**, 022509.

Reiman, A. 1996 Singular surfaces in the open field line region of a diverted tokamak. *Phys. Plasmas* **3**, 906.

Roeder, R. K. W., Rapoport, B. I. and Evans, T. E. 2003 Explicit calculations of homoclinic tangles in tokamaks. *Phys. Plasmas* **10**, 3796.

Schelin, A. B., Caldas, I. L., Viana, R. L. and Benkadda, S. 2011 Collisional effects in the tokamap. *Phys. Lett. A* **376**, 24.

Schmitz, O. et al. 2008 Aspects of three-dimensional transport for ELM control experiments in ITER-similar shape plasmas at low collisionality in DIII-D. *Plasma Phys. Control. Fusion* **50**, 124029.

Viana, R. L., da Silva, E. C., Kroetz, T., Caldas, I. L., Roberto, M. and Sanjuan, M. A. F. 2010 Fractal structures in nonlinear plasma physics. *Phil. Trans. R. Soc. A* **369**, 371.

Wingen, A., Evans, T. E. and Spatschek, K. H. 2009a Footprint structures due to resonant magnetic perturbations in DIII-D. *Phys. Plasmas* **16**, 042504.

Wingen, A., Evans, T. E. and Spatschek, K. H. 2009b High resolution numerical studies of separatrix splitting due to non-axisymmetric perturbation in DIII-D. *Nucl. Fusion* **49**, 055027.